UV Laser Photocarrier Radiometry of c-Silicon with Surface Thin Hydrogenated Amorphous Si Film

A. Melnikov, A. Mandelis, B. Halliop & N. P. Kherani

International Journal of Thermophysics
Journal of Thermophysical Properties and Thermophysics and Its Applications

ISSN 0195-928X
Volume 36
Combined 5-6

Int J Thermophys (2015) 36:1037-1044
DOI 10.1007/s10765-015-1835-1

Volume 36 • Numbers 5–6 • May–June 2015

International Journal of Thermophysics

ICPPP-17 Special Issue

IJOT • 10765 • ISSN 0195-928X
36(5–6) 809–1366 (2015)

Your article is protected by copyright and all rights are held exclusively by Springer Science +Business Media New York. This e-offprint is for personal use only and shall not be self-archived in electronic repositories. If you wish to self-archive your article, please use the accepted manuscript version for posting on your own website. You may further deposit the accepted manuscript version in any repository, provided it is only made publicly available 12 months after official publication or later and provided acknowledgement is given to the original source of publication and a link is inserted to the published article on Springer's website. The link must be accompanied by the following text: "The final publication is available at link.springer.com".

Springer

Author's personal copy

Int J Thermophys (2015) 36:1037–1044
DOI 10.1007/s10765-015-1835-1

UV Laser Photocarrier Radiometry of c-Silicon with Surface Thin Hydrogenated Amorphous Si Film

A. Melnikov · A. Mandelis · B. Halliop · N. P. Kherani

Received: 19 November 2013 / Accepted: 7 January 2015 / Published online: 23 January 2015
© Springer Science+Business Media New York 2015

Abstract Photocarrier radiometry (PCR) with 355 nm laser excitation was used for the study of c-Si covered with intrinsic thin hydrogenated amorphous Si (i-a-Si:H) on one, or both, sides, with thicknesses ranging from 10 nm to 90 nm. Short wavelength excitation allows one to resolve the contribution of the upper i-a-S layer to the PCR signal due to the very small absorption depth (tens of nm) of the excitation beam. As a result, fundamental transport parameters of the composite structure can be evaluated from the PCR frequency dependence. A theoretical model has been developed to describe the diffuse carrier density wave (CDW) in this two-layer system. The model of the one-dimensional CDW fields for composite electronic solids involves front, interface, and back surface recombination velocities, the diffusion coefficient, recombination lifetimes in the upper and lower layers, and the unoccupied trap density at the interface. Simulations of the transport parameter influence on the PCR signal were performed, and the theoretical model was able to describe the experimental data accurately, therefore, making it possible to evaluate the transport parameters of i-a-Si:H and c-Si as well as to elucidate the role of interface electronic traps in the PCR frequency dependence under short wavelength excitation.

Keywords Heterojunction · Photocarrier radiometry · Transport parameters · Two-layer model

A. Melnikov · A. Mandelis (✉)
Department of Mechanical and Industrial Engineering, Center for Advanced Diffusion-Wave Technologies (CADIFT), University of Toronto, Toronto, ON M5S 3G8, Canada
e-mail: mandelis@mie.utoronto.ca

A. Mandelis · B. Halliop · N. P. Kherani
Electrical and Computer Engineering, University of Toronto, Toronto, ON M5S 3G4, Canada

Author's personal copy

1 Introduction

Non-contact characterization of semiconductor materials with a submicron surface layer is important for optoelectronic device fabrication and optimization. In particular, heterostructures with nanometer-thick hydrogenated amorphous silicon overlayers are widely used in the production of high-efficiency photovoltaic devices [1]. Various methods have been used for the evaluation of transport parameters of the overlayer and substrate. Among them, photothermal and luminescence techniques have been shown to be effective [2–5]. However, the simultaneous determination of all four transport parameters of the overlayer and substrate remains difficult, especially in the case of the trap presence at the interface and/or the passivating surface layer. Detailed theoretical descriptions of a carrier density wave (CDW) in a two-layer composite have been developed [6]. The influence of the interface traps on the CDW has been considered in [7]. In this work, we present a one-dimensional (1-D) two-layer CDW model taking into account the effects of the unoccupied trap density at the interface and its application for the evaluation of the transport parameters of the i-α-Si:H thin overlayer and the c-Si substrate.

2 Experimental Apparatus and Procedures

A 355 nm laser was used in experiments as a photocarrier excitation source. The beam was harmonically modulated using an acousto-optic modulator in the frequency range of 0.01 kHz to 100 kHz. A long-pass filter LP1000 in front of the InGaAs detector prevented laser beam leakage onto the detector. The photocarrier radiometry (spectrally gated modulated photoluminescence) signal was collected, collimated, and focused on the detector with two off-axis paraboloidal mirrors. The signal from the detector was demodulated by a lock-in amplifier. The samples consisted of 290 μm thick CZ silicon wafers, in which i-a-Si:H nanolayers were deposited. The thicknesses of i-a-Si:H were 10 nm, 30 nm, and 90 nm for wafers #437, #438, and #439, respectively. 30 nm i-a-Si:H was deposited on four quadrants of another wafer (#451) (both sides, front side, back side, and no deposition, respectively) using masks.

3 Results and Discussion

The theoretical description of a 1-D CDW in a two-layer composite is based on the carrier diffusion-wave equations and is given in [6]. Modified boundary conditions exist at the interface to take into account the presence of traps there [7]:

$$D_1 \frac{\mathrm{d}}{\mathrm{d}x} N_1(x,\omega)\,|_{x=0} = S_1 N_1(0,\omega),\;\; N_1(L_1,\omega) - N_T(L_1) = N_2(L_1,\omega), \quad (1)$$

$$-D_1 \frac{\mathrm{d}}{\mathrm{d}x} N_1(x,\omega)\,|_{x=L_1} + D_2 \frac{\mathrm{d}}{\mathrm{d}x} N_2(x,\omega)\,|_{x=L_1} = S_i f n_T,\;\; -D_2 \frac{\mathrm{d}}{\mathrm{d}x} N_2(x,\omega)\,|_{x=L_2} = S_2 N_2(L_2,\omega), \quad (2)$$

Author's personal copy

where $\sigma_1 = \sqrt{\frac{1+i\omega\tau_1}{D_1\tau_1}}$, $\sigma_2 = \sqrt{\frac{1+i\omega\tau_2}{D_2\tau_2}}$, and $N_T(L_1) = fn_T$. Here N_1, D_1, τ_1, and β_1 are, respectively, the excess CDW concentration, ambipolar diffusion coefficient, excess carrier lifetime, and absorption coefficient in layer 1. N_2, D_2, τ_2, and β_2 are the respective quantities in layer 2. S_1, S_i, and S_2 are front surface, interface, and back surface recombination velocities. n_T is the trap density at the interface, $N_T(L_1)$ is the number density of free (unoccupied) traps, and f is the fraction of free trap states. The solutions for the coupled carrier density-wave equations subject to the boundary conditions (Eqs. 1 and 2) are

$$N_1(x,\omega) = A_1\cosh(\sigma_1 x) + B_1\sinh(\sigma_1 x) + \frac{I_0(1-R)\beta_1 e^{-\beta_1 x}}{2D_1(\sigma_1^2-\beta_1^2)}, \tag{3}$$

$$N_2(x,\omega) = A_2\cosh(\sigma_2 x) + B_2\sinh(\sigma_2 x) + \frac{I_0(1-R)\beta_2 e^{-\beta_1 L_1} e^{-\beta_2(x-L_1)}}{2D_2(\sigma_2^2-\beta_2^2)}. \tag{4}$$

Expressions for the constants A_1, B_1, A_2, and B_2 can be determined from the boundary conditions. The PCR signal is proportional to the CDW depth integral and can be expressed as

$$S_{PCR}(\omega) = C_L\left[\int_0^{L_1} N_1(x,\omega)dx + \int_{L_1}^{L_2} N_2(x,\omega)dx\right], \tag{5}$$

where C_L is constant which depends on instrumental factors and the radiative recombination efficiencies in the composite.

The effects of the unoccupied trap density on the carrier density amplitude and phase depth distribution and the corresponding CDW integral amplitude and phase on frequency are simulated and shown in Fig. 1a, b and c, d, respectively. An increase in the unoccupied trap density leads to a decrease of the carrier density amplitude in the substrate, while the carrier density amplitude in the overlayer remains practically the same. These trends clearly show that the substrate integral contribution to the CDW integral decreases with the increased free trap density compared with the overlayer integral. As a result, the frequency dependence of the CDW integral shows a decrease in the amplitude and phase minimum and a shift to lower frequencies with an increase in the unoccupied trap density. The phase minimum is the result of the balance between a trend for a larger phase lag with increased frequency due to the finite recombination lifetime of photocarriers mostly in the substrate and a counter-trend for a shorter phase lag due to the increased trapping rates closer to the surface (at the interface) and domination by short lifetime carriers within the overlayer with carrier losses at the interface. The effects of the upper layer thickness on the carrier density depth distribution and the corresponding frequency dependence of the CDW integral are presented in Fig. 1e, f and g, h, respectively. A thickness increase leads to a decrease of the carrier density amplitude in the substrate due to the substantial reduction of their density at the interface and, as result, to a decrease of the CDW integral amplitude and the appearance of a minimum in the phase frequency dependence. Similar to the foregoing discussion, the contribution of the upper layer becomes significant and the phase minimum appears. As the upper layer thickness increases, the phase minimum

Author's personal copy

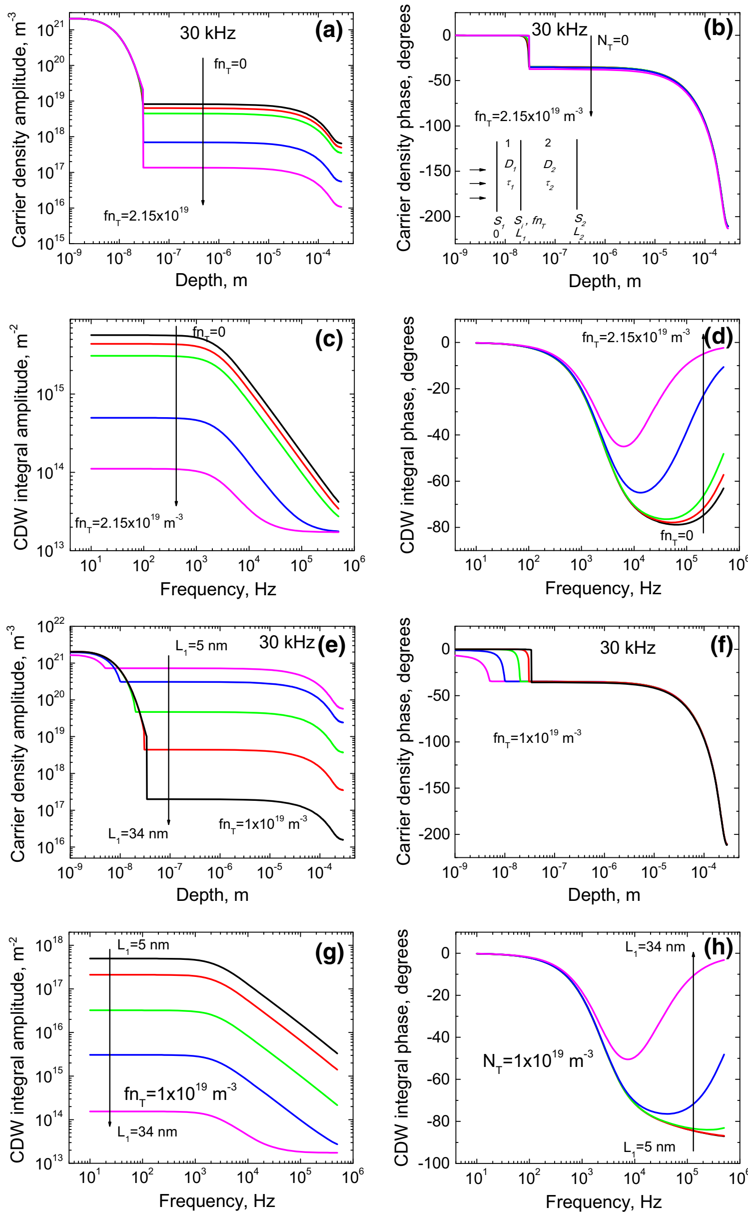

Fig. 1 Carrier density (a) amplitude and (b) phase depth distributions at frequency of 30 kHz and corresponding dependences of CDW integral (c) amplitude and (d) phase on frequency at various unoccupied trap densities, fn_{T}: 0, $5\times10^{18}\,\mathrm{m}^{-3}$, $1\times10^{19}\,\mathrm{m}^{-3}$, $2\times10^{19}\,\mathrm{m}^{-3}$, and $2.15\times10^{19}\,\mathrm{m}^{-3}$. Carrier density (e) amplitude and (f) phase depth distributions at frequency of 30 kHz and corresponding dependences of CDW integral (g) amplitude and (h) phase on frequency at $fn_{\mathrm{T}}=1\times10^{19}\,\mathrm{m}^{-3}$ for upper layer thickness L_1: 5 nm, 10 nm, 20 nm, 30 nm, and 34 nm. Simulation parameters: $I_0=8.5\times10^{22}\,\mathrm{m}^{-2}\cdot\mathrm{s}^{-1}$, $R=0.549$, $L_1=3\times10^{-8}\,\mathrm{m}$, $L_2=2.9\times10^{-4}\,\mathrm{m}$, $\beta_1=5\times10^{8}\,\mathrm{m}^{-1}$, $\beta_2=1.05\times10^{8}\,\mathrm{m}^{-1}$, $\tau_1=1.5\times10^{-9}\,\mathrm{s}$, $\tau_2=3\times10^{-4}\,\mathrm{s}$, $D_1=2\times10^{-8}\,\mathrm{m}^2\cdot\mathrm{s}^{-1}$, $D_2=8\times10^{-4}\,\mathrm{m}^2\cdot\mathrm{s}^{-1}$, $S_1=4\,\mathrm{m}\cdot\mathrm{s}^{-1}$, $S_{\mathrm{i}}=2\,\mathrm{m}\cdot\mathrm{s}^{-1}$, $S_2=1\,\mathrm{m}\cdot\mathrm{s}^{-1}$. Inset (b) is a schematic configuration of a two-layer optoelectronic solid

Author's personal copy

decreases and shifts to a lower frequency. The effects of the carrier recombination lifetime in the upper layer and in the substrate on the frequency dependences of the CDW integral are shown in Fig. 2a, b and c, d, respectively. The increase of the carrier recombination lifetime in the upper layer leads to a drastic amplitude increase of the CDW integral and an increase of the phase minimum with a shift to a higher frequency up to saturation at 90° (Fig. 2a, b). This is caused by the domination of substrate contributions to the CDW integral with an increase in the number of carriers reaching the interface which enhances carrier density growth in the substrate. The low-frequency "knee" in the amplitude and phase dependences retain the same position which is determined by transport parameters in the substrate. The increase of the carrier recombination lifetime in the substrate leads to an increase of the CDW integral amplitude and a shift of the "knee" in the amplitude and phase dependences to a lower frequency (Fig. 2c, d) as expected. A clearly defined phase minimum is observed. Furthermore, the simulation shows [7] that the effect of the back surface recombination velocity increase is similar to that observed with a decreased bulk recombination lifetime and points to an equivalence between the depth-integrated effects of the substrate lifetime decrease and back surface recombination velocity increase. It is further observed that the high-frequency phase upturn is not affected by the value of S_2.

The experimental PCR frequency scans of the quadrants of the Si wafer (i-a-Si:H deposited on both sides; on the front side only; and without i-a-Si:H deposition) are shown in Fig. 2e, f. The presence of the 30 nm hydrogenated amorphous silicon layer leads to the appearance of the pronounced minimum in the phase frequency dependence, but no minimum appears without this layer. Because the optical absorption length of Si at 355 nm is only ~10 nm [8], free photocarrier excitation originates mainly in the hydrogenated amorphous layer. The forward diffusion from this layer is the major source of carriers in the substrate along with direct excitation due to transmitted attenuated UV flux. The PCR amplitude of the two-side-deposited Si quadrant is significantly larger than the front-side-only deposited quadrant. This is due to the significant reduction of recombination on the back surface of the former Si quadrant at passivation by i-a-Si:H, which in turn leads to a higher CDW density in the bulk of the substrate c-Si and a concomitant reduction in the density of unoccupied traps at the front interface due to their neutralization (occupation). This double effect leads to a significant increase of the carrier density in the substrate, which, in turn, leads to a lifetime increase in the substrate due to trap neutralization in the bulk. The mean value results of multi-parameter fits according to the theoretical model with their standard deviations for front-side- and two-side-deposited quadrants are presented in Table 1, and confirm the described mechanism. PCR frequency scans of Si wafers deposited with 10 nm, 30 nm, and 90 nm thicknesses of i-a-Si:H on one front surface, respectively, are shown in Fig. 2g, h. The phase minimum appears only for upper layer thicknesses above 10 nm. It shifts to a lower frequency and decreases with increasing layer thickness as predicted by the theoretical model. The amplitude also decreases with increasing layer thickness following the theory. The mean value fit parameters with their standard deviations for the substrate and upper layer of the tested wafers are shown in Table 1. The i-a-Si:H layer thickness change on the front surface from 10 nm to 90 nm does not lead to any noticeable

Author's personal copy

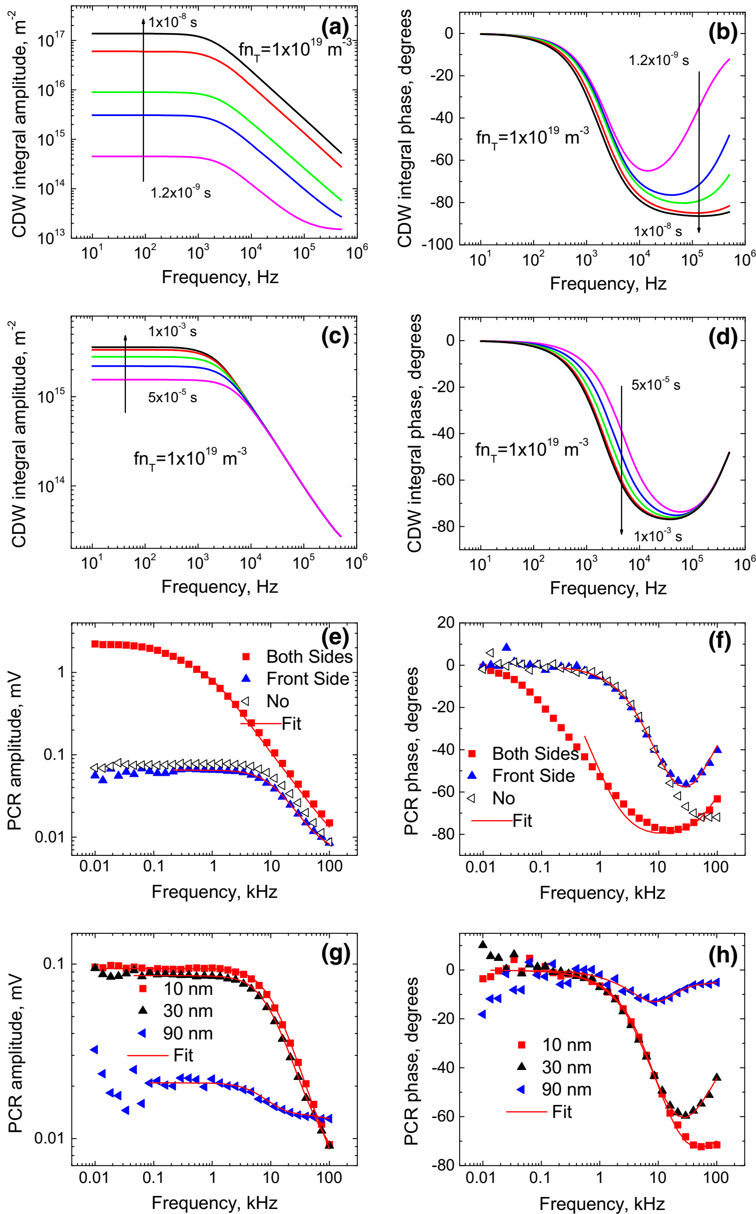

Fig. 2 (a, b) Dependence of the CDW integral on frequency at $fn_T = 1 \times 10^{19}$ m^{-3} for recombination carrier lifetimes in the upper layer τ_1: 1.2×10^{-9} s, 1.5×10^{-9} s, 2×10^{-9} s, 5×10^{-9} s, and 1×10^{-8} s for $\tau_2 = 3 \times 10^{-4}$ s; (c, d) for recombination carrier lifetimes in the substrate τ_2: 5×10^{-5} s, 1×10^{-4} s, 2×10^{-4} s, 5×10^{-4} s, 1×10^{-3} s for $\tau_1 = 1.5 \times 10^{-9}$ s. Other simulation parameters are as in Fig. 1. (e, f) Experimental PCR frequency scans in quadrants of c–Si wafer #451 with deposited 30 nm i–aSi:H on both sides, only front side, and without deposition; (g, h) and of silicon wafers #437, #438, #439 with deposited i-a-Si:H on one front side with thicknesses 10 nm, 30 nm, and 90 nm

Author's personal copy

Table 1 Mean and standard deviation of evaluated transport parameters of the front surface i-a-Si:H layer and the substrate

Fitted parameter	#451 30 nm a-Si on both sides	#451 30 nm a-Si on front side	#437 10 nm a-Si on front side	#438 30 nm a-Si on front side	#439 90 nm a-Si on front side
τ_2 (s)	1.4×10^{-3}	5.8×10^{-4}	6.1×10^{-4}	5.4×10^{-4}	5.8×10^{-4}
	$\pm 2 \times 10^{-4}$	$\pm 2.2 \times 10^{-4}$	$\pm 1.2 \times 10^{-4}$	$\pm 8.6 \times 10^{-5}$	$\pm 2.3 \times 10^{-4}$
D_2 ($m^2 \cdot s^{-1}$)	7.03×10^{-4}	7.9×10^{-4}	8.8×10^{-4}	6.4×10^{-4}	7.9×10^{-4}
	$\pm 2.4 \times 10^{-6}$	$\pm 9.1 \times 10^{-5}$	$\pm 1.3 \times 10^{-4}$	$\pm 1.9 \times 10^{-5}$	$\pm 6.7 \times 10^{-5}$
S_i ($m \cdot s^{-1}$)	3.1 ± 2.1	2.6 ± 1.3	9.5 ± 0.45	3.4 ± 2.4	5.6 ± 2.8
S_1 ($m \cdot s^{-1}$)	4.6 ± 2.7	5 ± 3.2	9.6 ± 0.56	7.6 ± 3.2	6 ± 2.1
S_2 ($m \cdot s^{-1}$)	0.2 ± 0.2	221 ± 194	190 ± 105	282 ± 187	250 ± 74
D_1 ($m^2 \cdot s^{-1}$)	7.4×10^{-9}	8.1×10^{-8}	5.4×10^{-8}	3.3×10^{-7}	1×10^{-7}
	$\pm 4.7 \times 10^{-9}$	$\pm 1.8 \times 10^{-8}$	$\pm 1.6 \times 10^{-8}$	$\pm 1.1 \times 10^{-7}$	$\pm 3.5 \times 10^{-8}$
τ_1 (s)	5.1×10^{-9}	1.4×10^{-9}	1.2×10^{-9}	1.5×10^{-9}	2.9×10^{-9}
	$\pm 3.3 \times 10^{-9}$	$\pm 5 \times 10^{-10}$	$\pm 3 \times 10^{-10}$	$\pm 3.9 \times 10^{-10}$	$\pm 1.1 \times 10^{-9}$
β_1 (m^{-1})	3×10^{8}	2.5×10^{8}	4.6×10^{8}	3.9×10^{8}	4×10^{8}
	$\pm 1 \times 10^{8}$	$\pm 1.1 \times 10^{8}$	$\pm 3 \times 10^{7}$	$\pm 3.1 \times 10^{8}$	$\pm 1.1 \times 10^{8}$
fn_T (m^{-3})	5.6×10^{19}	2.2×10^{20}	4.0×10^{20}	2.9×10^{20}	2.9×10^{20}
	$\pm 3.7 \times 10^{19}$	$\pm 9.5 \times 10^{19}$	$\pm 6.5 \times 10^{19}$	$\pm 1.9 \times 10^{20}$	$\pm 6.4 \times 10^{19}$

changes in substrate transport parameters or the lifetime and diffusion coefficient of the i-a-Si:H layer. The fitted results show that the transport parameters of the i-a-Si:H layer are significantly lower than the corresponding parameters of the substrate for all samples.

4 Conclusion

The obtained experimental and simulated PCR results show that carrier transport in the i-a-Si:H layer–c-Si substrate system is controlled by the upper layer and/or interface defects. The theoretical model was applied to the evaluation of the transport properties of a i-a-Si:H overlayer deposited on c-Si as well as those of the substrate, using a multi-parameter fitting procedure. Carrier recombination lifetimes, diffusion coefficients, front and back surface and interface recombination velocities, as well as effective unoccupied trap densities at the interface, and the absorption coefficient of the i-a-Si:H layer were measured from the PCR amplitude and phase frequency dependences measured under excitation with a modulated UV laser beam.

Acknowledgments A. Mandelis is grateful to NSERC for a Discovery Grant, to the Canada Foundation for Innovation (CFI) for equipment grants, and to the Canada Research Chairs Program of the Government of Canada.

Author's personal copy

References

1. T. Mishima, M. Taguchi, H. Sakata, E. Maruyama, Sol. Energy Mater. Sol. Cells **95**, 18 (2011)
2. A. Salnick, A. Mandelis, J. Appl. Phys. **80**, 5278 (1996)
3. S. Ilahi, N. Yacoubi, F. Genty, J. Appl. Phys. **113**, 183705 (2013)
4. B. Li, D. Shaughnessy, A. Mandelis, J. Batista, J. Appl. Phys. **95**, 7832 (2004)
5. S. Tardon, R. Brüggemann, J. Phys. D **43**, 115102 (2010)
6. A. Mandelis, *Diffusion-Wave Fields: Mathematical Methods and Green Functions* (Springer, New York, 2001). chap. 9
7. A. Melnikov, A. Mandelis, B. Halliop, N.P. Kherani, J. Appl. Phys. **114**, 244506 (2013)
8. M.A. Green, Sol. Energy Mater. Sol. Cells **92**, 1305 (2008)